Composites Part B 128 (2017) 19–29

Contents lists available at ScienceDirect

Composites Part B

journal homepage: www.elsevier.com/locate/compositesb

Stability of magnetoactive composites with periodic microstructures undergoing finite strains in the presence of a magnetic field

Artemii Goshkoderia, Stephan Rudykh*

Department of Aerospace Engineering, Technion – Israel Institute of Technology, Haifa 32000, Israel

ARTICLE INFO

Article history:
Received 23 February 2017
Received in revised form
23 May 2017
Accepted 8 June 2017
Available online 20 June 2017

Keywords:
Magnetorheological elastomers
Stability
Composites
Finite deformation
Microstructure

ABSTRACT

We investigate the macroscopic magnetomechanical instabilities in magnetorheological elastomer (MRE) composites undergoing finite strains in the presence of a magnetic field. In particular, we identify the unstable domains for MRE composites with periodically distributed circular and elliptical inclusions embedded in a soft matrix. We use the isotropic Langevin model for magnetic behavior, to account for the initial (linear) susceptibility and saturation magnetization of the magnetoactive inclusions. We analyze the influence of the applied magnetic field and finite strains, as well as particle shape and material properties, on the stability of the MRE composites. We find that the stable and unstable domains can be significantly tuned by the applied magnetic field, depending on deformation, microstructure and magnetic properties of the inclusions such as initial susceptibility and saturation magnetization.

1. Introduction

Magnetorheological elastomers (MREs) are materials that can change their mechanical behavior in response to application of an external magnetic field. Recently, these materials have attracted significant attention due to their relatively simple, remote and reversible principle of actuation making them suitable for various applications. Potential applications include remotely controlled actuators [12,61], variable-stiffness devices, tunable vibration absorbers and damping components [15,28,33,41], noise barrier system [23] and sensors [62] among others.

Typically, MREs are composite materials that consist of magnetizable particles embedded in a soft matrix material. A polymeric matrix material (e.g. silicone rubber) in its liquid state before polymerization, is mixed with magnetizable particles (of micro or even nano size) such as iron (cobalt, nickel, or Terfenol-D) magnetizable powder [35]. Curing in the presence of a magnetic field causes the iron particles to arrange into chain like structures resulting in an anisotropic behavior. If magnetic field is not applied during polymerization, the magnetizable particles remain randomly distributed in the resulting magnetoactive material.

Magnetomechanical properties of parallel chains of magnetically permeable spherical particles have been examined by Jolly et al. [35]. The investigation of magnetostriction of composites made with randomly distributed particles subjected to ultrahigh magnetic fields was carried out by Bednarek [3]. The magnetostriction of random and chain structured MREs was determined experimentally by Ginder and co-workers [27,29]. Lanotte et al. [40] investigated the effect of particle rotation on the average magnetization of the composite. In turn, Diguet et al. [17] have examined composite shape effect in the magnetostriction and Keip and Rambausek [37] in the experimental characterization of ferromagnetic composites.

The theory of electro- and magneto-elastic macroscopic behavior of continuum was proposed by Truesdell and Toupin [64]. This theory has been recently reformulated and further developed by Brigadnov and Dorfmann [8], Dorfmann and Ogden [20,21], Bustamante et al. [10], Vu and Steinmann [65], Melnikov and Ogden [43], and Destrade and Ogden [16]. In parallel, significant efforts have been made towards the development and implementation of the non-linear magneto- [34,38] and electroelasticity [13] framework (which is described by a similar set of equations) into numerical schemes [30,39,46,58]. An analytical approach for estimating the response and effective properties of MREs with random distribution of magnetoactive particles has been developed by Ponte Castañeda and Galipeau [51]. By comparing the responses of MREs with random and periodic distributions of magnetoactive particles, Galipeau et al. [24] showed that MAEs with similar microstructures may posses very different magnetomechanical

* Corresponding author.
E-mail address: rudykh@technion.ac.il (S. Rudykh).

http://dx.doi.org/10.1016/j.compositesb.2017.06.014
1359-8368/

properties. Moreover, the periodic microstructures can be tailored to produce significant enhancement in the coupled properties (see, for example, Rudykh et al. [57] for mathematically analogous dielectric elastomer composites). Bustamante and Merodio [11] extended the analysis of constitutive restrictions proposed for isotropic nonlinearly elastic materials to transversely isotropic elastic solids and isotropic magneto-sensitive elastomers.

However, the heterogeneity of the composite material may give rise to the instability phenomenon. The phenomenon has been historically considered as a failure, which should be predicted and avoided. Thus, the topic of elastic instabilities in composite materials under purely mechanical loadings has been investigated thoroughly (see for example, Biot [7], Hill and Hutchinson [32], Triantafyllidis and Maker [63], Geymonat et al. [26], Michel et al. [47], Merodio and Ogden [44], and Rudykh and deBotton [56]). More recently, the phenomenon of elastic instability in nonlinear materials has developed into new directions, in which the instabilities are used to trigger microstructure transformations Mullin et al. [48], Bertoldi et al. [5], Li et al. [42], Gao and Li [25], Slesarenko and Rudykh [59,60], Budday et al. [9] and to gain enriched control over switchable functionalities [2,4,54].

The instability analysis for the "purely" mechanical case, has been extended to study the onset of coupled magnetomechanical instabilities in isotropic MREs focusing on surface instabilities of homogeneous magnetoactive half-space [50] and failure modes of a rectangular MRE block undergoing plane strain deformation in the presence of a magnetostatic field [36]. Danas and Triantafyllidis [14] have examined surface instabilities in film/substrate structures.Rudykh and Bertoldi [52] analyzed the macroscopic instabilities in anisotropic MREs by employing an exact solution for finitely deformed MRE laminates. A mathematically analogous problem of macroscopic and microscopic instabilities in dielectric elastomer laminates has been examined by Bertoldi and Gei [6], Rudykh and deBotton [55], Rudykh et al. [53].

In this study, we perform an analysis of macroscopic magnetomechanical instabilities in MRE composites with periodically arranged active particles embedded in a matrix. In particular, we focus on the stability of MRE periodic composites with circular and elliptical inclusions. We developed a numerical finite element based code to analyze the magnetomechanical instabilities of finitely deformed MREs. By means of the numerical simulations, we identify the unstable domains for finitely deformed MRE composites in the presence of a magnetic field. We analyze the influence of the magnetic field, pre-stretch, microstructure and material parameters on MRE composite stability.

The work is structured as follows: Sec. 2 presents the theoretical background for the finitely deformed magnetorheological elastomers and magnetomechanical instability analysis. The numerical simulations, including the magnetomechanical periodic boundary conditions, and the procedure for determination of the onset of the magnetomechanical instability are described in Sec. 3. In Sec. 4, we apply the stability analysis to identify the unstable domains for the MRE composites with periodically distributed circular (4.1) and elliptical (4.2) inclusions embedded in a matrix, and analyze the influence of various parameters on the stability of MREs. Sec. 5 concludes the paper with a summary and a discussion.

2. Theoretical background

2.1. Magnetorheological elastomers

We consider a magnetoelastic deformable solid that occupies a region $\mathscr{B}_0$ (and $\mathscr{B}$) with a boundary $\partial\mathscr{B}_0$ (and $\partial\mathscr{B}$) of outward normal $\mathbf{N}^0$ (and $\mathbf{N}$) in the reference (and current) configuration. The Cartesian position vector of a material point in the reference configuration of a body is $\mathbf{X}$ and its position vector in the deformed configuration is $\mathbf{x}$. We introduce a mapping vector function $\boldsymbol{\chi}$ such that

$$\mathbf{x} = \boldsymbol{\chi}(\mathbf{X}). \tag{1}$$

The deformation gradient is defined as

$$\mathbf{F} = \frac{\partial \boldsymbol{\chi}(\mathbf{X})}{\partial \mathbf{X}}. \tag{2}$$

The ratio between the volumes in the current and reference configurations is $J \equiv \det\mathbf{F} > 0$. The magnetoelastic solid satisfies the conservation of mass $\rho_0 = \rho J$, where ρ_0 and ρ are the densities in the reference and current configurations, respectively.

We consider a quasi-static deformation in the absence of an electric field, electrical charges or electric currents within the material. Consequently, Maxwell equations and boundary conditions take the form

$$\mathrm{div}\mathbf{B} = 0 \quad \text{and} \quad \mathrm{curl}\mathbf{H} = 0, \quad \text{in} \quad \mathscr{B}, \tag{3}$$

$$[\![\mathbf{B}]\!]\cdot\mathbf{N} = 0 \quad \text{and} \quad [[\mathbf{H}]] \times \mathbf{N} = 0, \quad \text{in} \quad \partial\mathscr{B}, \tag{4}$$

where $\mathbf{B}$ is the magnetic induction and $\mathbf{H}$ is the magnetic intensity in the current configuration and $\mathbf{N} = \mathbf{F}^{-T}\mathbf{N}^0$. We distinguish between the differential operators div(•),curl(•) and grad(•) in the current configuration and the operators Div(•),Curl(•) and Grad(•) in the reference configuration. The magnetization is defined via the standard relation

$$\mathbf{M} = \frac{\mathbf{B}}{\mu_0} - \mathbf{H} \quad \text{in} \quad \mathscr{B}, \quad \mathbf{M} = 0 \quad \text{in} \quad \mathscr{R}^3\backslash\mathscr{B}, \tag{5}$$

where μ_0 is the magnetic permeability of vacuum and $\mathscr{R}^3\backslash\mathscr{B}$ is a region of surrounding space of non-magnetized material (e.g. vacuum). For later use, it is convenient to introduce the scalar magnetic potential U_m, such that

$$\mathbf{H} = -\mathrm{grad}U_m \quad \text{in} \quad \mathscr{B}, \tag{6}$$

$$[\![U_m]\!] = 0 \quad \text{in} \quad \partial\mathscr{B}. \tag{7}$$

The referential magnetic intensity, magnetic induction and magnetization are related to their counterpart in the deformed configuration via

$$\mathbf{H}^0 = \mathbf{F}^{\mathrm{T}}\mathbf{H}, \quad \mathbf{B}^0 = J\mathbf{F}^{-1}\mathbf{B} \quad \text{and} \quad \mathbf{M}^0 = \mathbf{F}^{\mathrm{T}}\mathbf{M}. \tag{8}$$

Equations (5)–(7) can be written in the reference configuration as

$$\mathrm{Div}\mathbf{B}^0 = 0 \quad \text{and} \quad \mathrm{Curl}\mathbf{H}^0 = 0, \quad \text{in} \quad \mathscr{B}_0, \tag{9}$$

$$[\![\mathbf{B}^0]\!]\cdot\mathbf{N}^0 = 0 \quad \text{and} \quad [\![\mathbf{H}^0]\!] \times \mathbf{N}^0 = 0, \quad \text{in} \quad \partial\mathscr{B}_0, \tag{10}$$

$$\mathbf{M}^0 = J^{-1}\frac{\mathbf{C}\mathbf{B}^0}{\mu_0} - \mathbf{H}^0 \quad \text{in} \quad \mathscr{B}_0, \quad \mathbf{M}^0 = 0 \quad \text{in} \quad \mathscr{R}^3\backslash\mathscr{B}_0, \tag{11}$$

where $\mathbf{C} = \mathbf{F}^T\mathbf{F}$ is the right Cauchy-Green strain tensor. We follow the analysis proposed by Dorfmann and Ogden [18,19] and consider magnetoelastic solids whose constitutive relation is given in terms of a scalar-valued energy-density function $\Psi(\mathbf{F}, \mathbf{H}^0)$ such that

$$\mathbf{P}=\frac{\partial\Psi(\mathbf{F},\mathbf{H}^0)}{\partial\mathbf{F}}\quad\text{and}\quad\mathbf{B}^0=-\frac{\partial\Psi(\mathbf{F},\mathbf{H}^0)}{\partial\mathbf{H}^0},\tag{12}$$

where $\mathbf{P}$ is the total first Piola-Kirchhoff stress tensor. The corresponding equations for an incompressible material are

$$\mathbf{P}=\frac{\partial\Psi(\mathbf{F},\mathbf{H}^0)}{\partial\mathbf{F}}-p\mathbf{F}^{-T}\quad\text{and}\quad\mathbf{B}^0=-\frac{\partial\Psi(\mathbf{F},\mathbf{H}^0)}{\partial\mathbf{H}^0},\tag{13}$$

where p is an unknown Lagrange multiplier. For an isotropic magnetoelastic material, an energy-density function Ψ can be expressed as a function of the six invariants

$$\Psi\left(\mathbf{F},\mathbf{H}^0\right)=\Psi(I_1,\ I_2,\ I_3,\ I_{4m},\ I_{5m},\ I_{6m}),\tag{14}$$

where

$$I_1=\mathrm{Tr}\mathbf{C},\quad I_2=\frac{1}{2}\left(I_1^2-\mathrm{Tr}\left(\mathbf{C}^2\right)\right),\quad I_3=\det\mathbf{C},\tag{15}$$

$$I_{4m}=\mathbf{H}^0\cdot\mathbf{H}^0,\quad I_{5m}=\mathbf{H}^0\cdot\mathbf{C}^{-1}\mathbf{H}^0,\quad I_{6m}=\mathbf{H}^0\cdot\mathbf{C}^{-2}\mathbf{H}^0.\tag{16}$$

In the absence of body forces the equilibrium equation and boundary condition in the reference configuration take the form

$$\mathrm{Div}\mathbf{P}=0\quad\text{in}\quad\mathscr{B}_0,\quad\text{and}\quad[\![\mathbf{P}]\!]\cdot\mathbf{N}^0=0\quad\text{in}\quad\partial\mathscr{B}_0,\tag{17}$$

or in the deformed configuration

$$\mathrm{div}\mathbf{T}=0\quad\text{in}\quad\mathscr{B},\quad\text{and}\quad[\![\mathbf{T}]\!]\cdot\mathbf{N}=0\quad\text{in}\quad\partial\mathscr{B},\tag{18}$$

where the Cauchy stress tensor is related to the first Piola-Kirchhoff stress tensor via $\mathbf{T}=J^{-1}\mathbf{P}\mathbf{F}^T$.

2.2. Incremental equations

Following the approach recently developed to investigate instabilities in electroactive composites [22,53,55], we derive the governing equations for the incremental deformations superimposed upon a given state of finite deformation in the presence of a magnetic field. The incremental equations are

$$\mathrm{Div}\dot{\mathbf{P}}=0,\quad\mathrm{Div}\dot{\mathbf{B}}^0=0\quad\text{and}\quad\mathrm{Curl}\dot{\mathbf{H}}^0=0,\tag{19}$$

where $\dot{\mathbf{P}}$, $\dot{\mathbf{B}}^0$ and $\dot{\mathbf{H}}^0$ are the incremental changes in $\mathbf{P}$, $\mathbf{B}^0$ and $\mathbf{H}^0$, respectively. The linearized expressions for the incremental changes in the first Piola-Kirchhoff stress tensor and magnetic induction are

$$\dot{P}_{ij}=\mathscr{A}^0_{ijkl}\dot{F}_{kl}+\mathscr{M}^0_{ijk}\dot{H}^0_k\quad\text{and}\quad-\dot{B}^0_i=\mathscr{M}^0_{jki}\dot{F}_{jk}+\mathscr{H}^0_{ij}\dot{H}^0_j,\tag{20}$$

where the tensors of the magnetoelastic moduli are defined as

$$\mathscr{A}^0_{i\alpha k\beta}=\frac{\partial^2\Psi}{\partial F_{i\alpha}\partial F_{k\beta}},\quad\mathscr{M}^0_{i\alpha\beta}=\frac{\partial^2\Psi}{\partial F_{i\alpha}\partial H^0_\beta}\quad\text{and}\quad\mathscr{H}^0_{\alpha\beta}=\frac{\partial^2\Psi}{\partial H^0_\alpha\partial H^0_\beta}.\tag{21}$$

For an incompressible material, Eq. $(20)_1$ modifies as

$$\dot{P}_{ij}=\mathscr{A}^0_{ijkl}\dot{F}_{kl}+\mathscr{M}^0_{ijk}\dot{H}^0_k-\dot{p}F^{-T}_{ij}+pF^{-1}_{jk}\dot{F}_{kl}F^{-1}_{li},\tag{22}$$

where $\dot{p}$ is an incremental change in p. The components of the magnetoelastic moduli in the current and reference configurations are related via

$$\mathscr{A}_{ijkl}=J^{-1}F_{j\alpha}F_{l\beta}\mathscr{A}^0_{i\alpha k\beta},\quad\mathscr{M}_{ijk}=J^{-1}F_{j\alpha}F_{k\beta}\mathscr{M}^0_{i\alpha\beta}\quad\text{and}\quad\mathscr{H}_{ij}=J^{-1}F_{i\alpha}F_{j\beta}\mathscr{H}^0_{\alpha\beta}.\tag{23}$$

It can be shown that these moduli posses the symmetries

$$\mathscr{A}_{ijkl}=\mathscr{A}_{klij},\quad\mathscr{M}_{ijk}=\mathscr{M}_{jik}\quad\text{and}\quad\mathscr{H}_{ij}=\mathscr{H}_{ji}.\tag{24}$$

Let $\dot{\mathbf{T}}$, $\dot{\mathbf{B}}$ and $\dot{\mathbf{H}}$ denote the 'push-forward' counterparts of $\dot{\mathbf{P}}$, $\dot{\mathbf{B}}^0$ and $\dot{\mathbf{H}}^0$, respectively. These incremental changes are given by

$$\dot{\mathbf{T}}=J^{-1}\dot{\mathbf{P}}\mathbf{F}^T,\quad\dot{\mathbf{B}}=J^{-1}\mathbf{F}\dot{\mathbf{B}}^0\quad\text{and}\quad\dot{\mathbf{H}}=\mathbf{F}^{-T}\dot{\mathbf{H}}^0.\tag{25}$$

We introduce the notation for the incremental displacement $\mathbf{v}=\dot{\mathbf{x}}$ and recall that $\dot{\mathbf{F}}=(\mathrm{grad}\,\mathbf{v})\mathbf{F}$. By substitution of (22) and (23) into (25), we obtain

$$\dot{T}_{ij}=\mathscr{A}_{ijkl}v_{k,l}+\mathscr{M}_{ijk}\dot{H}_k-\dot{p}\delta_{ij}+pv_{j,i}\quad\text{and}\quad-\dot{B}_i=\mathscr{M}_{jki}v_{j,k}+\mathscr{H}_{ij}\dot{H}_j.\tag{26}$$

In the current configuration the incremental equation (19) take the form

$$\mathrm{div}\dot{\mathbf{T}}=0,\quad\mathrm{div}\dot{\mathbf{B}}=0\quad\text{and}\quad\mathrm{curl}\dot{\mathbf{H}}=0.\tag{27}$$

By using eqs. $(26),(27)_1,(27)_2$ we obtain

$$\mathscr{A}_{ijkl}v_{k,lj}+\mathscr{M}_{ijk}\dot{H}_{k,j}-\dot{p}_{,i}=0\quad\text{and}\quad\mathscr{M}_{jki}v_{j,ki}+\mathscr{H}_{ij}\dot{H}_{j,i}=0.\tag{28}$$

2.3. Macroscopic instabilities

Long-wavelength or macroscopic instabilities are known to be of particular prominence in nonlinear fiber composites [44,45]. In the mechanics of non-linear composites it has been shown that macroscopic instabilities occur when the homogenized properties lose strong ellipticity [26]. Extending the formulation presented by Hill and Hutchinson [32] for the purely mechanical case and following the recent works by Destrade and Ogden [16], Rudykh and deBotton [55], and Rudykh et al. [53], we seek for solution of Eq. (28) in the form

$$v_i=\tilde{v}_i f(\mathbf{n}\cdot\mathbf{x}),\quad\dot{p}=\tilde{q}g(\mathbf{n}\cdot\mathbf{x}),\quad\dot{H}_i=\tilde{h}_i g(\mathbf{n}\cdot\mathbf{x}),\tag{29}$$

where f is a continuous and sufficiently differentiable function, $\mathbf{n}=n_1\bar{\mathbf{e}}_1+n_2\bar{\mathbf{e}}_2+n_3\bar{\mathbf{e}}_3$ is a unit vector; $\tilde{v}_i$, $\tilde{h}_i$ and $\tilde{q}$ are incremental macroscopic quantities independent of $\mathbf{x}$.

For a 2-D case, equation $(27)_3$ reduces to

$$\dot{H}_{2,1}-\dot{H}_{1,2}=0.\tag{30}$$

By using $(29)_3$ together with (30), we find that

$$\tilde{h}_1=\xi^{-1}\tilde{h}_2,\tag{31}$$

where $\xi\equiv n_2/n_1$. Next, we recall that the incompressibility constraint implies that $\mathrm{div}\mathbf{v}=0$, and for the plane-strain condition $v_{1,1}+v_{2,2}=0$. Then, from Eq. $(29)_1$ we have

$$\tilde{v}_1=-\xi\tilde{v}_2.\tag{32}$$

Substituting Eqs. (29), (31) and (32) into (28), we obtain the sextic polynomial equation (for details see Refs. [52,53])

$$\Gamma_6\xi^6+\Gamma_5\xi^5+\Gamma_4\xi^4+\Gamma_3\xi^3+\Gamma_2\xi^2+\Gamma_1\xi+\Gamma_0=0, \tag{33}$$

where the coefficients Γ_i are presented in Appendix A.

The existence of a non-trivial real solution of the polynomial Eq. (33) is associated with the onset of instability along a magneto-mechanical loading path. In the following, Eq. (33) serves as the onset of instability condition for considered MRE composites.

2.4. Soft ferromagnetism

Typical MRE composites consist of magnetically susceptible particles embedded in a soft elastomeric matrix. The particles are usually made of magnetic materials such as iron, nickel, cobalt or Terfenol-D. For simplicity, we assume these ferromagnetic materials to be soft (in the magnetic sense), so that the hysteresis effects can be neglected and the particles assumed to be large compared to the typical magnetic domain size. We note that in our model, we assume the particles to be isotropic, i.e. we consider them to be superparamagnetic and, thus, neglecting demagnetization effects [1]. The possible influence of the effect on the stability of MREs is not considered here. As a result, the material behavior can be described by a single-valued constitutive response. Although other models can be used, in this work we use the isotropic Langevin model for the magnetic behavior of the particles. The corresponding magnetic energy is

$$\rho\Phi(\mathbf{B})=-\frac{\mu_0 m_s^2}{3\chi}\left[\ln\left(\sinh\left[\frac{3\chi|\mathbf{B}|}{\mu_0 m_s}\right]\right)-\ln\left(\frac{3\chi|\mathbf{B}|}{\mu_0 m_s}\right)\right], \tag{34}$$

where m_s is the saturation magnetization, χ is the initial susceptibility and $|\mathbf{B}|$ is the absolute value of the magnetic induction vector. The magnetization is defined by the following relation

$$\mathbf{M}(\mathbf{B})=-\rho\frac{\partial\Phi}{\partial\mathbf{B}}=\frac{m_s}{|\mathbf{B}|}\left[\coth\left(\frac{3\chi|\mathbf{B}|}{\mu_0 m_s}\right)-\frac{\mu_0 m_s}{3\chi|\mathbf{B}|}\right]\mathbf{B}. \tag{35}$$

Note that equation (35) implies that magnetization and magnetic field vectors are collinear. Thus, the interaction of the magnetic field and the magnetic moment does not result in appearance of the magnetic torque under this assumption. The magnetic force in the particles, which is proportional to the rate of change of the magnetic field, is nonzero only if the magnetic field is inhomogeneous.

Alternatively, the magnetic energy function can be expressed in terms of $\mathbf{H}$, thus the magnetic energy Eq. (34) can be expressed in the following form

$$\rho\Phi\left(\mathbf{H}^0\right)=-\frac{\mu_0 m_s^2}{3\chi}\left[\ln\left(\sinh\left[\frac{3\chi\sqrt{\mathbf{H}^0\cdot\mathbf{C}^{-1}\mathbf{H}^0}}{m_s}\right]\right)-\ln\left(\frac{3\chi\sqrt{\mathbf{H}^0\cdot\mathbf{C}^{-1}\mathbf{H}^0}}{m_s}\right)\right], \tag{36}$$

which is a function of the invariant I_{5m} defined in Eq. $(16)_2$; note that usually the active particles are significantly stiffer than the matrix, and deformations that the particles experience are negligible. Typical values of saturation magnetization of some magnetoactive materials are summarized in Table 1.

The magnetic field - induction dependence $\mathbf{H}(\mathbf{B})$ is presented in Fig. 1(a). The dash-dotted, continuous and dashed curves are for the saturation magnetization $\mu_0 m_s = 10, 5$ and 2 T, respectively. Note that the dependence is highly nonlinear for relatively small magnetic fields, when the *initial* susceptibility plays a crucial role. However, we observe the linear behavior of the $\mathbf{H}(\mathbf{B})$ curve for relatively high magnetic fields, after the saturation magnetization is achieved. Examples of the dependence of magnetization on magnetic field are shown in Fig. 1(b). The dash-dotted, continuous and dashed curves are for the initial susceptibilities $\chi = 0.999, 0.75$ and 0.5, respectively. The magnetization increases fast and then, reaches a saturation value. The saturation magnetization is achieved faster for higher values of initial susceptibility.

Table 1
Typical values of $\mu_0 m_s$ for different magnetoactive materials.

Inclusions	Cobalt-iron alloy	High purity iron	Steels	Cast iron	Nickel alloys
$\mu_0 m_s$(Tesla)	2.35	2.16	2.00 −2.15	1.7	0.77

3. Analysis

In this section, we describe the numerical analysis for determining the onset of magnetomechanical instabilities in periodic two-phase composites undergoing finite deformations in the presence of a magnetic field. We consider magnetoelastic material that occupies a domain Ω_0 (in the undeformed configuration), which is made of two distributed (homogeneous) phases, occupying subdomains $\Omega_0^{(r)}$ $(r = 1, 2)$ in Ω_0. An example of an MRE composite subjected to a magnetic field is shown in Fig. 2. Note that the position of the magnet poles does not change with the deformation, thus the applied magnetic field is the same in the deformed and undeformed state. However, local magnetic field can be different in the deformed and undeformed state. The analysis is implemented in the finite element code COMSOL Multiphysics 4.2a.[1]

The energy-density function of a two-phase composite is

$$\Psi\left(\overline{\mathbf{F}},\mathbf{X},\overline{\mathbf{H}}^0\right)=\varphi^{(1)}(\mathbf{X})\Psi^{(1)}\left(\mathbf{F},\mathbf{H}^0\right)+\varphi^{(2)}(\mathbf{X})\Psi^{(2)}\left(\mathbf{F},\mathbf{H}^0\right), \tag{37}$$

where the characteristic function defined in each phase r is

$$\varphi^{(r)}(\mathbf{X})=\begin{cases}1, & \text{if } \mathbf{X}\in\mathscr{B}_0^{(r)};\\ 0, & \text{otherwise.}\end{cases} \tag{38}$$

The volume fraction of the r-phase is

$$c^{(r)}=\int_{\mathscr{B}_0}\varphi^{(r)}(\mathbf{X})\,dV. \tag{39}$$

The volume fractions are related via

$$c^{(1)}+c^{(2)}=1. \tag{40}$$

Thus, we numerically solve the following equations

$$\begin{cases}\text{div}\mathbf{T}=0, \mathbf{x}\in\mathscr{B};\\ \text{div}(\text{grad}U_m+\mathbf{M})=0, \mathbf{x}\in\mathscr{B}.\end{cases} \tag{41}$$

The magnetomechanical loading is imposed by applying periodic boundary conditions for both the displacement (u_1, u_2) and magnetic potential (U_m) (see [31] in the mechanical context). The applied average deformation gradient and magnetic intensity are defined as

[1] In our numerical simulation, the problem has been solved on the meshes with the number of elements $N_e \approx 7200$ (for the lowest volume fraction $c^{(i)} = 0.05$ the number of elements is $N_e = 7070$ and $N_e = 7470$ for the highest one $c^{(i)} = 0.3$); the mesh sensitive analysis has been performed.

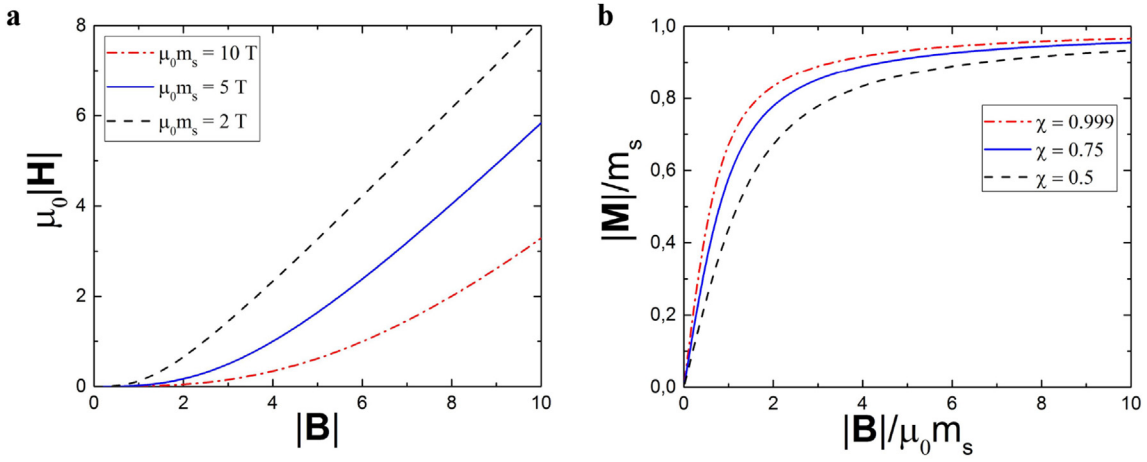

Fig. 1. Dependence of magnetic intensity (a) and magnetization (b) on magnetic field; initial susceptibility is $\chi = 0.999$ in (a). The illustration is given for the undeformed case ($\mathbf{F} = \mathbf{I}$).

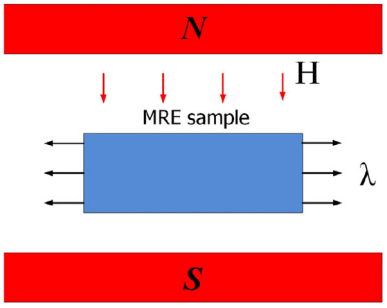

Fig. 2. Typical experimental setup for study of MREs.

$$\overline{\mathbf{F}} = \frac{1}{V}\int_{\mathscr{B}_0} \mathbf{F}(\mathbf{X})\, dV \quad \text{and} \quad \overline{\mathbf{H}} = \frac{1}{V}\int_{\mathscr{B}} \mathbf{H}(\mathbf{x})\, dV, \tag{42}$$

respectively. The average Cauchy and 1st Piola-Kirchhoff stress tensor together with magnetic induction are

$$\overline{\mathbf{T}} = \frac{1}{V}\int_{\mathscr{B}} \mathbf{T}(\mathbf{x})\, dV, \quad \overline{\mathbf{P}} = \frac{1}{V}\int_{\mathscr{B}_0} \mathbf{P}(\mathbf{X})\, dV \quad \text{and} \quad \overline{\mathbf{B}} = \frac{1}{V}\int_{\mathscr{B}} \mathbf{B}(\mathbf{x})\, dV, \tag{43}$$

respectively.

In the 2-D case the integration is performed over the unit cell, which occupies the domain

$$0 \le X_1 \le a \quad \text{and} \quad 0 \le X_2 \le a, \tag{44}$$

in the reference configuration. These periodic boundary conditions are:

The top ($X_2 = a$) and bottom ($X_2 = 0$) sides are related via

$$\begin{cases} u_2^B = u_2^T + (\overline{F}_{22} - 1)a, \\ u_1^B = u_1^T + \overline{F}_{12}a, \\ U_m^B(x_1, 0) = U_m^T(x_1, a) + \overline{H}_2 a. \end{cases} \tag{45}$$

The right ($X_1 = a$) and left ($X_1 = 0$) sides are related via

$$\begin{cases} u_1^L = u_1^R + (\overline{F}_{11} - 1)a, \\ u_2^L = u_2^R + \overline{F}_{21}a, \\ U_m^L(0, x_2) = U_m^R(a, x_2) + \overline{H}_1 a. \end{cases} \tag{46}$$

In the considered plane-strain case, we also assume the absence of a magnetic field in the $\mathbf{X}_3$ direction. Application of the periodic boundary conditions allows us to determine the solution along a magneto-mechanical loading path. Here we consider the magnetomechanical loading defined as

$$\overline{\mathbf{F}}^{[0]} = \overline{\lambda}\mathbf{e}_1 \otimes \mathbf{e}_1 + \overline{\lambda}^{-1}\mathbf{e}_2 \otimes \mathbf{e}_2 + \mathbf{e}_3 \otimes \mathbf{e}_3 \quad \text{and} \quad \overline{\mathbf{H}}^{[0]} = \overline{H}_1\mathbf{e}_1 + \overline{H}_2\mathbf{e}_2. \tag{47}$$

Note that the applied average magnetic field does not change with the deformation. This corresponds to the relevant MRE experimental settings (see. Fig. 2). However, the local distributions of the magnetic field can change with applied deformation. The average response of the periodic composites is calculated by integration over the corresponding unit cell according to Eq. $(43)_1$ and $(43)_2$. The primary solution is valid until a possible instability point along the magnetomechanical loading.

To identify the onset of coupled magnetomechanical instabilities, we utilize the critical condition (33). The analysis of the magnetomechanical stability of MRE composites requires determination of the instantaneous tensors of the magnetoelastic moduli $\mathscr{A}_{ijkl}$, $\mathscr{M}_{ijk}$ and $\mathscr{H}_{ij}$. To this end we perform a set of incremental changes in deformation $\dot{\mathbf{F}}$ and magnetic field $\dot{\mathbf{H}}$ from a finitely deformed state in the presence of a magnetic field (see Fig. 3). These incremental changes lead to a macroscopic response of the MRE composite, resulting in variations in the average nominal stress and magnetic induction. The following five small amplitude tests are performed as follows

$$\overline{\mathbf{F}}^{[1]} = \overline{\lambda}\mathbf{e}_1 \otimes \mathbf{e}_1 + \delta\overline{\gamma}\mathbf{e}_1 \otimes \mathbf{e}_2 + \overline{\lambda}^{-1}\mathbf{e}_2 \otimes \mathbf{e}_2 + \mathbf{e}_3 \otimes \mathbf{e}_3 \quad \text{and} \quad \overline{\mathbf{F}}^{[2]} = \overline{\lambda}\mathbf{e}_1 \otimes \mathbf{e}_1 + \overline{\lambda}^{-1}\mathbf{e}_2 \otimes \mathbf{e}_2 + \delta\overline{\gamma}\mathbf{e}_2 \otimes \mathbf{e}_1 + \mathbf{e}_3 \otimes \mathbf{e}_3, \tag{48}$$

$$\overline{\mathbf{F}}^{[3]} = \left(\overline{\lambda} + \delta\overline{\lambda}\right)\mathbf{e}_1 \otimes \mathbf{e}_1 + \left(\overline{\lambda} + \delta\overline{\lambda}\right)^{-1}\mathbf{e}_2 \otimes \mathbf{e}_2 + \mathbf{e}_3 \otimes \mathbf{e}_3, \tag{49}$$

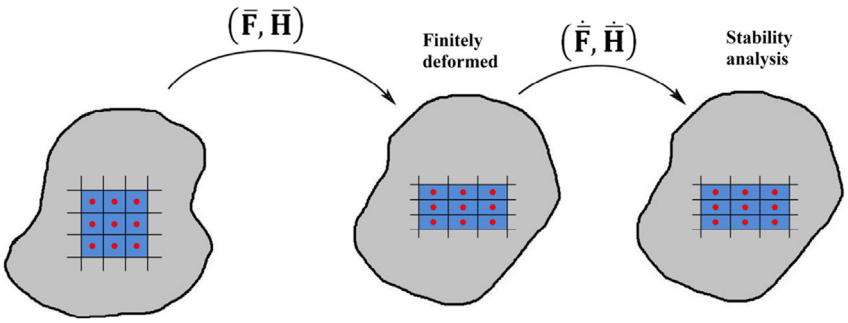

Fig. 3. Small incremental changes in terms of deformation gardient $\dot{\mathbf{F}}$ and magnetic field $\dot{\mathbf{H}}$ are superimposed on a finitely deformed solid in the presence of a magnetic field..

$$\overline{\mathbf{H}}^{[1]} = (\overline{H}_1 + \delta\overline{H})\mathbf{e}_1 + \overline{H}_2\mathbf{e}_2 \quad \text{and} \quad \overline{\mathbf{H}}^{[2]} = \overline{H}_1\mathbf{e}_1 + (\overline{H}_2 + \delta\overline{H})\mathbf{e}_2, \tag{50}$$

where $\delta\overline{\gamma}$, $\delta\overline{\lambda}$ and $\delta\overline{H}$ are sufficiently small quantities. By performing these tests and making use of the relations (20),(26) and (23), the magnetoelastic moduli are determined. The corresponding equations for the magnetoelastic moduli are

$$\begin{aligned}\mathscr{A}^0_{ijkl} &= \frac{\delta\overline{P}^{[m,0]}_{ij}}{\delta\overline{F}^{[m]}_{kl}} = \frac{\overline{P}_{ij}\left(\overline{\mathbf{F}}^{[m]}, \overline{\mathbf{H}}^{[0]}\right) - \overline{P}_{ij}\left(\overline{\mathbf{F}}^{[0]}, \overline{\mathbf{H}}^{[0]}\right)}{\overline{F}^{[m]}_{kl} - \overline{F}^{[0]}_{kl}} \\ &= \frac{\overline{P}_{ij}\left(\overline{\mathbf{F}}^{[m]}, \overline{\mathbf{H}}^{[0]}\right) - \overline{P}_{ij}\left(\overline{\mathbf{F}}^{[0]}, \overline{\mathbf{H}}^{[0]}\right)}{\delta\overline{\gamma}}, k \neq l, m = 1, 2;\end{aligned} \tag{51}$$

$$\mathscr{A}_{ijkl} = \overline{F}^{[0]}_{jj}\overline{F}^{[0]}_{ll}\mathscr{A}^0_{ijkl}, \ \text{(no summation)}, k \neq l; \tag{52}$$

$$\begin{aligned}\mathscr{M}_{ijk} &= \frac{\delta\overline{T}^{[0,n]}_{ij}}{\delta\overline{H}^{[n]}_k} = \frac{\overline{T}_{ij}\left(\overline{\mathbf{F}}^{[0]}, \overline{\mathbf{H}}^{[n]}\right) - \overline{T}_{ij}\left(\overline{\mathbf{F}}^{[0]}, \overline{\mathbf{H}}^{[0]}\right)}{\overline{H}^{[n]}_k - \overline{H}^{[0]}_k} \\ &= \frac{\overline{T}_{ij}\left(\overline{\mathbf{F}}^{[0]}, \overline{\mathbf{H}}^{[n]}\right) - \overline{T}_{ij}\left(\overline{\mathbf{F}}^{[0]}, \overline{\mathbf{H}}^{[0]}\right)}{\delta\overline{H}}, n = 1, 2;\end{aligned} \tag{53}$$

$$\begin{aligned}\mathscr{H}_{ij} &= -\frac{\delta\overline{B}^{[0,n]}_i}{\delta\overline{H}^{[n]}_j} = -\frac{\overline{B}_i\left(\overline{\mathbf{F}}^{[0]}, \overline{\mathbf{H}}^{[n]}\right) - \overline{B}_i\left(\overline{\mathbf{F}}^{[0]}, \overline{\mathbf{H}}^{[0]}\right)}{\overline{H}^{[n]}_j - \overline{H}^{[0]}_j} \\ &= -\frac{\overline{B}_i\left(\overline{\mathbf{F}}^{[0]}, \overline{\mathbf{H}}^{[n]}\right) - \overline{B}_i\left(\overline{\mathbf{F}}^{[0]}, \overline{\mathbf{H}}^{[0]}\right)}{\delta\overline{H}}, n = 1, 2.\end{aligned} \tag{54}$$

Note that in Eq. (51) only shear tests $\overline{\mathbf{F}}^{[1]}$ and $\overline{\mathbf{F}}^{[2]}$ are applied, consequently $m = 1, 2$. To determine the components of magnetoelastic moduli $\mathscr{A}^0_{ijkk}$ (no summation), $i \neq j$, we use the symmetry $\mathscr{A}^0_{ijkk} = \mathscr{A}^0_{kkij}$ and apply Eq. (51) again. However, when $i = j$ and $k = l$, the components $\mathscr{A}^0_{iikk}$ (no summation) cannot be determined from the tension test (49). This is due to the fact that the following equation system stemming from Eq. (20)

$$\begin{cases}\delta\overline{P}^{[3,0]}_{11} = \mathscr{A}^0_{1111}\delta\overline{F}^{[3]}_{11} + \mathscr{A}^0_{1122}\delta\overline{F}^{[3]}_{22}, \\ \delta\overline{P}^{[3,0]}_{22} = \mathscr{A}^0_{2211}\delta\overline{F}^{[3]}_{11} + \mathscr{A}^0_{2222}\delta\overline{F}^{[3]}_{22},\end{cases} \tag{55}$$

does not have a solution for $\mathscr{A}^0_{1111}$, $\mathscr{A}^0_{2222}$, and $\mathscr{A}^0_{1122} = \mathscr{A}^0_{2211}$. Clearly, it is impossible to fully characterize the elastic properties of a material on the basis of plane tests alone [49]. However, the corresponding coefficients in the critical condition for the onset of instabilities (33) can be fully determined through certain combinations of the terms $\mathscr{A}^0_{iikk}$ (no summation). The procedure of determination these terms is presented in Appendix B.

By utilizing Eqs. (23),(24),(A.1),(51)–(54),(B.3)-(B.4) and (A.1) all the components of the magneto-elastic tensors required for calculating of the coefficients Γ_i can be determined. In order to perform the stability analysis, we evaluate the components of magnetoelastic moduli from the numerical tests, and, then, we check the condition for the onset of instability (33) at each point of the magnetomechanical loading path. Thus, the critical magnetic field and deformation are determined. Results of the stability analysis of specific periodic MRE composites are discussed in the next section.

4. Results

In this section, we consider MRE composites with periodically distributed stiff magnetizable particles embedded in a soft matrix. Representative 2-D MRE composites with circular and elliptical

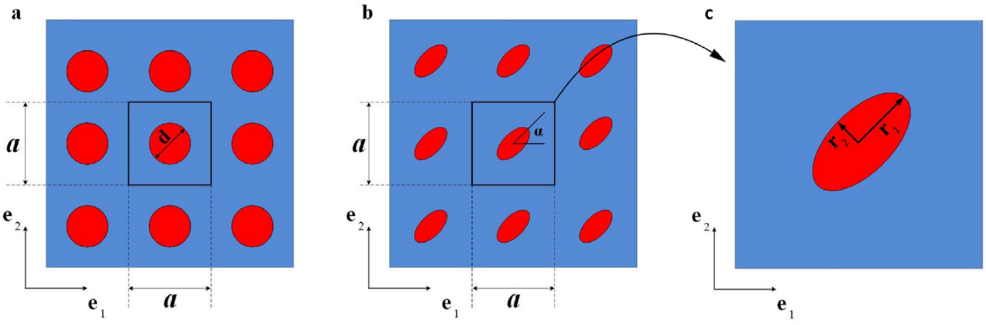

Fig. 4. Schematic representation of MRE composites with square periodic microstructures with circular (a) and elliptical (b) inclusions; the periodic unit cell (c).

inclusions are shown in Fig. 4(a) and (b). The energy densities of the corresponding phases are

$$\Psi^{(m)}=\frac{G^{(m)}}{2}(I_1-3)-G^{(m)}\ln J+\left(\frac{K^{(m)}}{2}-\frac{G^{(m)}}{3}\right)(J-1)^2-\frac{\mu_0 J}{2}I_{5m},$$
$$\Psi^{(i)}=\frac{G^{(i)}}{2}(I_1-3)-G^{(i)}\ln J+\left(\frac{K^{(i)}}{2}-\frac{G^{(i)}}{3}\right)(J-1)^2-\frac{\mu_0 J}{2}I_{5m}+\rho\Phi(I_{5m}), \tag{56}$$

where K is the bulk modulus, G is the shear modulus, μ_0 is relative permeability, ρ is the mass density of the inclusion material and the function $\Phi(I_{5m})$ is given in Eq. (36). The superscripts (m) and (i) denote matrix and inclusion phases, respectively. The invariants I_1 and I_{5m} are defined in Eqs.$(15)_1$ and$(16)_2$. In our numerical modeling we assign a high ratio of bulk to shear moduli, in particular $K/G=100$, to maintain a nearly incompressible behavior in each phase. The stiffness of the inclusions is reached by assigning a high ratio of shear moduli of the phases, namely $G^{(i)}/G^{(m)}=1000$.

4.1. MRE composites with periodically distributed circular inclusions

Here we examine the response of MRE composites with periodically distributed circular particles embedded in a soft matrix. A representative 2-D periodic composite with a square periodic unit cell with circular inclusions is shown in Fig. 4(a).

Fig. 5 shows the dependence of the critical stretch ratio λ_c, corresponding to the onset of macroscopic instability on the applied magnetic field in terms of the normalized magnetic intensity

$$\tilde{H}=\overline{H}_2\sqrt{\mu_0/G^{(m)}}. \tag{57}$$

Here and thereafter the magnetic intensity is applied in the $\mathbf{e}_2$ direction. The dash-dotted, continuous and dashed curves are for the MREs with the particle susceptibilities $\chi=0.999, 0.75$ and 0.5, respectively. The volume fraction of the magnetizable inclusion is $c^{(i)}=0.1$. The saturation magnetization is $\mu_0 m_s=2.16$ T. The arrows indicate transitions form stable to unstable domains. Fig. 5(a) is presented for the contraction ($\overline{\lambda}<1$), while Fig. 5(b) is presented for the extension ($\overline{\lambda}>1$). For the compression case ($\overline{\lambda}<1$), the critical stretch is found to increase fast and it reaches a maximum, and then decreases with a further increase in the magnetic intensity. This means that the MRE composite is first destabilized by the magnetic field up to some critical point $\overline{\lambda}_c=\overline{\lambda}_{c,max}$ (corresponding to the smallest critical strain level $\varepsilon_c=|\lambda_c-1|$) and then the magnetic field starts to stabilize the composite. MRE composites become more stable with a decrease in the initial susceptibility. The magnetic field corresponding to this maximum is highest in the case of the lowest initial susceptibility $\chi=0.5$ ($\tilde{H}\approx 3.8$). The dash-dotted curve, corresponding to the MRE with the highest considered initial susceptibility $\chi=0.999$ is above the continuous and dashed curves for all values of the applied magnetic intensity. When subjected to an extension, MREs also exhibit the switch in the role of the magnetic field on the stability (see Fig. 5(b)). We observe an increase in the critical stretch before a point $\tilde{H}\approx 2$ where the curve $\overline{\lambda}_c(\tilde{H})$ reaches a maximum. This increase is followed by a relatively fast decrease in the critical stretch as the magnetic field is further increased. An increase in initial susceptibility results in stabilizing effect in the case of extension. Notice that the value of the corresponding to the maximum is very close for the different MRE composites with different susceptibilities. However, in the case of extension ($\overline{\lambda}>1$), we observe the opposite effect, the magnetic field first stabilizes the composite up to some value, but then the composite is destabilized with a further increase in the magnetic field. The switch happens at the level of the magnetic field $\tilde{H}\approx 2$. The dash-dotted, continuous and dashed curves become very close for relatively high values of the applied magnetic field. This result is consistent with the fact, that for high values of the magnetic field, when saturation is achieved, the $\mathbf{H}(\mathbf{B})$ curve does not depend on *initial* susceptibility. We observe that the distance between the curves in Fig. 5 increases with an increase in the magnetic intensity up to $\tilde{H}\approx 3$ in the case of contraction, and $\tilde{H}\approx 2$ in the case of extension and then, this distance decreases with further increase in magnetic field. This behavior is very similar to the one observed in Fig. 1(b).

The dependence of the critical stretch on the magnetic intensity for MREs with different volume fractions of the inclusions is shown in Fig. 6. The saturation magnetization and initial susceptibility of the particles are $\mu_0 m_s=1.70$ T and $\chi=0.999$, respectively. The dash-dotted, continuous and dashed curves are for the volume fractions $c^{(i)}=0.3, 0.2$ and 0.1, respectively. Fig. 6(a) shows that the critical stretch increases and reaches a maximum at the magnetic intensity $\tilde{H}\approx 2.9$ and then decreases gradually with a further increase in the magnetic intensity. Consistent with the previous

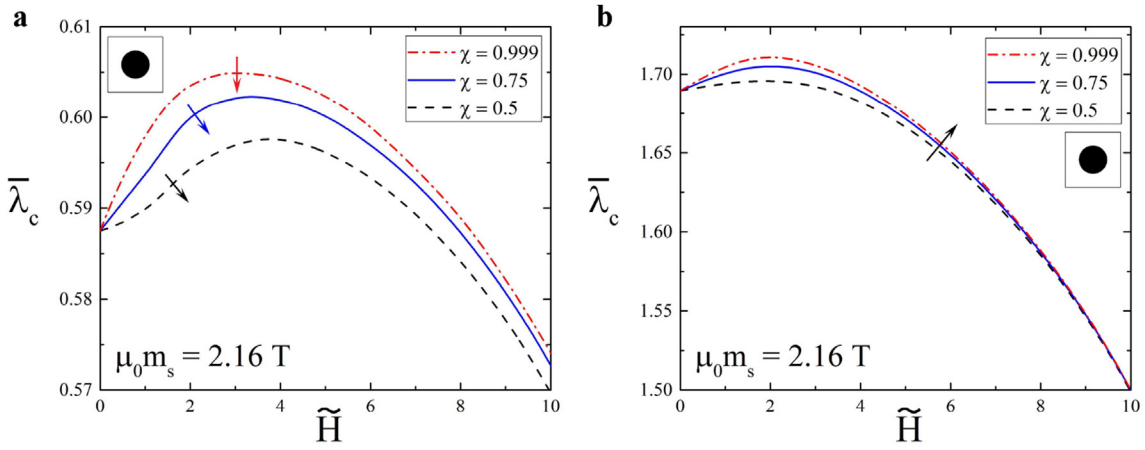

Fig. 5. Critical stretch vs magnetic intensity for MRE composites with the saturation magnetization $\mu_0 m_s=2.16$ T for the contraction (a) and extension (b). The volume fraction of the inclusion is $c^{(i)}=0.1$.

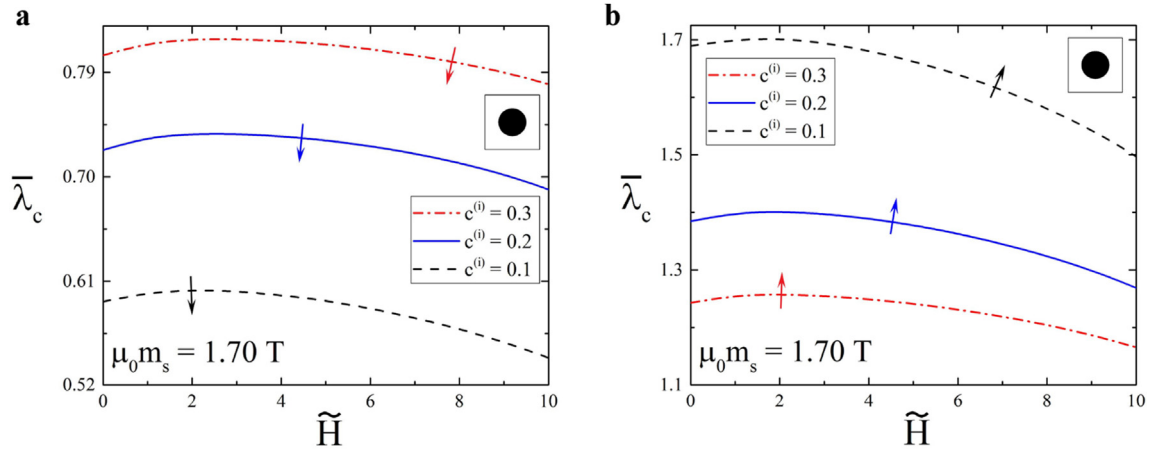

Fig. 6. Critical stretch vs magnetic intensity for MRE composites with the saturation magnetization $\mu_0 m_s = 1.70$ T for the contraction (a) and extension (b). The initial susceptibility is $\chi = 0.999$.

observations, we find that the magnetic field destabilizes MRE composite until some maximum value of stretch, and then magnetic field starts to stabilize MRE composite. The opposite effect is shown in Fig. 6(b) when tension ($\overline{\lambda} > 1$) is applied. The critical stretch slightly increases up to some maximum, and then starts to decrease fast. The magnetic field has a significant effect on the critical stretch for the lowest volume fraction $c^{(i)} = 0.1$ ($\overline{\lambda}_c \in [1.69, 1.5]$), while for higher volume fractions the influence of the magnetic field decreases. In addition, MRE composites become more unstable with an increase in the volume fraction of the rigid inclusion phase. The dash-dotted curve, corresponding to the MRE with the highest volume fraction $c^{(i)} = 0.3$ is more close to the undeformed state ($\overline{\lambda} = 1$) than continuous and dashed curves for all values of the applied magnetic field. We observe that for the lowest volume fraction $c^{(i)} = 0.1$, the critical stretch (dashed curve in Fig. 6(b)) decreases faster than for other volume fractions. This means that at relative high magnetic fields, the effect of magnetic field on the stable domains is greater for the lowest volume fractions.

4.2. MRE composites with periodically distributed elliptical inclusions

Here we examine the stability of MREs with periodically distributed elliptical inclusions (see the illustration in Fig. 4(b) and (c)). The aspect ratio of the elliptical particles is defined as the ratio between the semi-major and the semi-minor axes $w = r_1/r_2$. The inclination angle α is defined as the angle between $\mathbf{e}_1$-direction and semi-major axis of the elliptical inclusions (Fig. 4(b)). Because of the symmetry of the unit cell, only inclination angles in the range $\alpha \in (0, \pi/2)$ need to be considered.

Fig. 7 shows the dependence of the critical stretch on the applied magnetic field (in terms of magnetic intensity $\tilde{H}$) for MREs with elliptical inclusions oriented perpendicularly to ($\alpha = 0$ in Fig. 7(a and b)), and aligned with the applied average magnetic field ($\alpha = \pi/2$ in Fig. 7(c and d)). The dash-dotted, continuous and dashed curves are for the particle susceptibilities $\chi = 0.999, 0.75$ and 0.5, respectively. The volume fraction of the magnetizable inclusion is $c^{(i)} = 0.05$. The saturation magnetization is $\mu_0 m_s = 2.16$ T. We observe that the magnetic field has similar effects on the critical stretch as in the case of the circular inclusions. In the case of contraction (Fig. 7(a),(c)), the MRE composite is first destabilized by a magnetic field up to some point and then, magnetic field starts to stabilize the MRE composites. In the case of extension (Fig. 7(b),(d)), we observe the opposite effect. Consistent with the previous observations, we find that an increase in initial susceptibility results in stabilizing (Fig. 7(b),(d)) and destabilizing (Fig. 7(a),(c)) effects. In the case of contraction ($\overline{\lambda} < 1$), we observe that the magnetic field influences the critical stretch more significantly if applied perpendicular to the semi-major axis of the elliptical inclusions. For example, for MREs with initial susceptibility $\chi = 0.999$, the difference is $\overline{\lambda}_{c,max} - \overline{\lambda}_c(\tilde{H} = 10) = 0.02$ for the magnetic field applied along the major axis of the elliptical inclusions (Fig. 7(a)), and it is $\overline{\lambda}_{c,max} - \overline{\lambda}_c(\tilde{H} = 10) = 0.029$ for the magnetic field applied perpendicularly to the major axis of the elliptical inclusions (Fig. 7(c)). The opposite trend is observed for the case of extension ($\overline{\lambda} > 1$); in particular, the difference $\overline{\lambda}_{c,max} - \overline{\lambda}_c(\tilde{H} = 10) = 0.333$ for the case when magnetic field is applied along the major axis of the elliptical inclusions (Fig. 7(b)), and the difference $\overline{\lambda}_{c,max} - \overline{\lambda}_c(\tilde{H} = 10) = 0.26503$ is smaller for case when the magnetic field is applied perpendicularly to the major axis of the elliptical inclusions (Fig. 7(d)).

The dependence of the critical stretch on the aspect ratio of the elliptical particles is shown in Fig. 8. The saturation magnetization of the particles is $\mu_0 m_s = 2.35$ T and initial susceptibility is $\chi = 0.999$. The applied normalized magnetic intensity is $\tilde{H} = 3$. The volume fraction is kept constant at the value $c^{(i)} = 0.2$. The dash-dotted, continuous and dashed curves are for the inclination angles of the elliptical inclusion $\alpha = \pi/6, \pi/12$ and 0, respectively. All curves intersect at the point $w = 1$, corresponding to the MREs with circular inclusions. We observe that for the aligned case, $\alpha = 0$ (dashed curves in Fig. 8), the critical stretch is an increasing function of the aspect ratio. This means that an increase in w leads to destabilization of MREs for compressive loading (Fig. 8(a)), and it stabilizes the MREs subjected to tension (Fig. 8(b)). The dependence of the critical stretch on the aspect ratio is almost linear in the case of contraction (Fig. 8(a)). However, the behavior changes drastically, when non-aligned cases are examined. For the inclination angles $\alpha = \pi/12, \pi/6$, the dependence of the critical stretch on the aspect ratio is characterized by a unique maximum for MREs under contraction (Fig. 8(a)) or minimum for the MREs under tension (Fig. 8(b)).

5. Conclusions

In this work, we examined the macroscopic stability of periodic

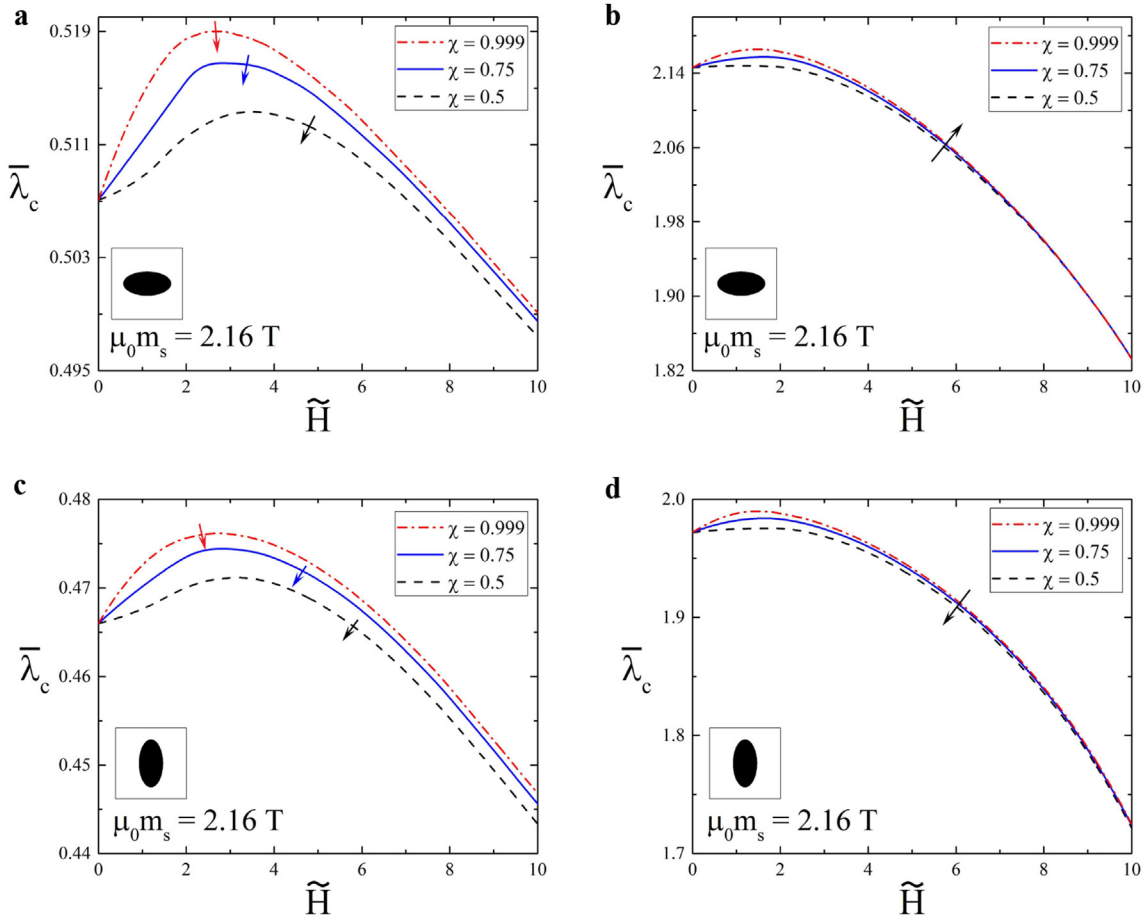

Fig. 7. Critical stretch vs magnetic intensity for MRE composites with the aspect ratio $w = 2$ and inclination angles of the elliptical inclusion $\alpha = 0$ (a,b) and $\alpha = \pi/2$ (c,d). The saturation magnetization is $\mu_0 m_s = 2.35$ T. The volume fraction of the inclusion is $c^{(i)} = 0.05$.

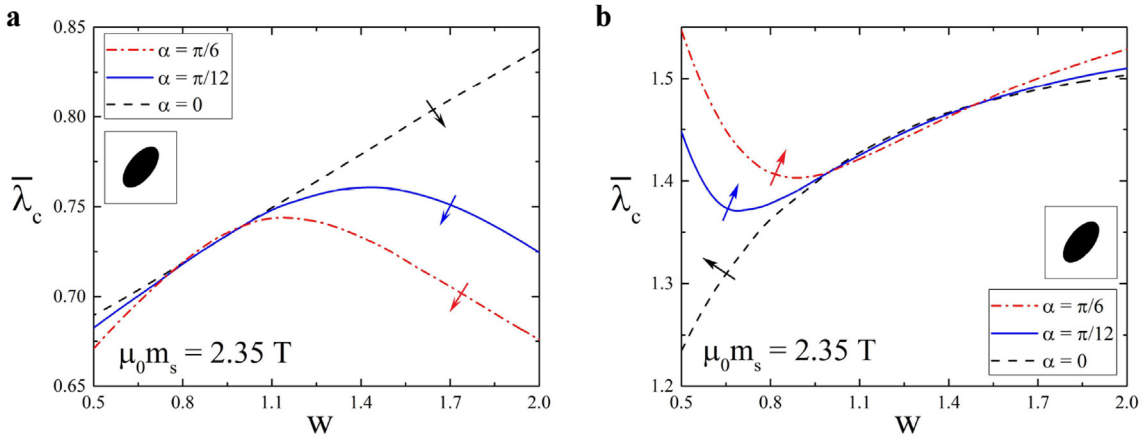

Fig. 8. Critical stretch vs aspect ratio for MREs composites with of elliptical inclusions; saturation magnetization $\mu_0 m_s = 2.35$ T and initial susceptibility $\chi = 0.999$; volume fraction of inclusions is $c^{(i)} = 0.2$. The applied dimensionless magnetic intensity is $\tilde{H} = 3$.

MRE composites subjected to finite strains in the presence of a magnetic field. Through the numerical evaluation of instantaneous magnetoelastic moduli, the unstable domains were determined for periodic MRE composites with circular and with elliptical inclusions periodically distributed within a soft matrix. We analyzed the influence of the magnetomechanical loading, geometrical and material parameters on the stability of the MRE composites with the particulate microstructures. We found that an increase in initial susceptibility of the particles resulted in a more stable behavior of the MRE composites subjected to magnetic field in the case of extension, and in a decreased stability in the case of contraction. Consistent with the isotropic Langevin model, for the MRE composites with circular inclusions, we found that initial susceptibility of the particles affects stable domains of MRE composites subjected to relatively low magnetic fields, while this effect significantly weakens at larger magnetic fields, when the saturation

magnetization is attained. We found that the effect of the relatively high magnetic fields on the stable/unstable domains is more significant for the MREs with lower volume fractions of magnetizable particles. The dependence of the critical stretch on the applied magnetic field is characterized by a unique extreme point, which is only slightly affected by a magnetic field in the case of extension. For MRE composites with elliptical inclusions, we found that the geometrical parameters of the inclusions such as inclination angle and aspect ratio significantly affect the stable/unstable domains. In particular, for the non-aligned cases, we found that the dependence of the critical stretch on the aspect ratio is characterized by a unique maximum in the case of contraction and minimum in the case of extension at a certain inclination angle. For the aligned case (when the semi-major axis coincided with the stretch direction), we observe that an increase in the aspect ratio leads to an increase in the critical stretch.

Acknowledgments

This research was supported by the Israel Science Foundation (grant 1550/15 and 19713/15). Stephan Rudykh gratefully acknowledges the support of Taub Foundation through the Horev Fellowship – Leaders in Science and Technology.

Appendix A

$$
\begin{aligned}
\Gamma_0 &= \mathscr{M}_{121}^2 - \mathscr{A}_{2121}\mathscr{H}_{11},\\
\Gamma_1 &= 2(-\mathscr{A}_{2121}\mathscr{H}_{12} + (\mathscr{A}_{1121} - \mathscr{A}_{2122})\mathscr{H}_{11}\\
&\quad + \mathscr{M}_{121}(\mathscr{M}_{221} + \mathscr{M}_{122} - \mathscr{M}_{111})),\\
\Gamma_2 &= -\mathscr{A}_{2121}\mathscr{H}_{22} + 4(\mathscr{A}_{1121} - \mathscr{A}_{2122})\mathscr{H}_{12}\\
&\quad - (\mathscr{A}_{1111} - 2\mathscr{A}_{1122} - 2\mathscr{A}_{1221} + \mathscr{A}_{2222})\mathscr{H}_{11}\\
&\quad - 2\mathscr{M}_{121}(\mathscr{M}_{112} + \mathscr{M}_{121} - \mathscr{M}_{222}) + (\mathscr{M}_{122} + \mathscr{M}_{221} - \mathscr{M}_{111})^2,\\
\Gamma_3 &= -2((\mathscr{A}_{1112} - \mathscr{A}_{1222})\mathscr{H}_{11} + (\mathscr{A}_{1111} - 2\mathscr{A}_{1122} - 2\mathscr{A}_{1221}\\
&\quad + \mathscr{A}_{2222})\mathscr{H}_{12} + (\mathscr{A}_{2122} - \mathscr{A}_{1121})\mathscr{H}_{22} + (\mathscr{M}_{121}\mathscr{M}_{122}\\
&\quad - (\mathscr{M}_{111} - \mathscr{M}_{122} - \mathscr{M}_{221})(\mathscr{M}_{112} + \mathscr{M}_{121} - \mathscr{M}_{222}))),\\
\Gamma_4 &= -(\mathscr{A}_{1111} - 2\mathscr{A}_{1122} - 2\mathscr{A}_{1221} + \mathscr{A}_{2222})\mathscr{H}_{22}\\
&\quad - 4(\mathscr{A}_{1112} - \mathscr{A}_{1222})\mathscr{H}_{12} - \mathscr{A}_{1212}\mathscr{H}_{11}\\
&\quad + (\mathscr{M}_{112} + \mathscr{M}_{121} - \mathscr{M}_{222})^2 + 2\mathscr{M}_{122}(\mathscr{M}_{111} - \mathscr{M}_{122} - \mathscr{M}_{221}),\\
\Gamma_5 &= 2((\mathscr{A}_{1222} - \mathscr{A}_{1112})\mathscr{H}_{22} - \mathscr{A}_{1212}\mathscr{H}_{12}\\
&\quad + \mathscr{M}_{122}(\mathscr{M}_{112} + \mathscr{M}_{121} - \mathscr{M}_{222})), \Gamma_6 = \mathscr{M}_{122}^2 - \mathscr{A}_{1212}\mathscr{H}_{22}.
\end{aligned}
\tag{A.1}
$$

Appendix B

The combinations $\mathscr{A}^0_{iikk}$ (no summation) can be obtained from the information provided by the tension test (49). The incompressibility constraint implies

$$\delta\overline{\mathbf{F}} : \overline{\mathbf{F}}^{-T} = 0. \tag{B.1}$$

For the tension test (49), the incompressibility constraint reads

$$\delta\overline{F}^{[3]}_{11} = -\delta\overline{F}^{[3]}_{22}\frac{\overline{F}^{[3]}_{11}}{\overline{F}^{[3]}_{22}} = -\frac{\delta\overline{F}^{[3]}_{22}}{\left(\overline{F}^{[3]}_{22}\right)^2}. \tag{B.2}$$

Thus, the combinations $(\mathscr{A}^0_{2222} - \mathscr{A}^0_{2211})$ and $(\mathscr{A}^0_{1111} - \mathscr{A}^0_{2211})$ can be determined by applying the tension test (49) together with $(23)_1$,(55) and (B.2). In particular, we obtain

$$
\begin{aligned}
\mathscr{A}^0_{2222} - \mathscr{A}^0_{2211} &= \overline{F}^{[0]}_{22}\overline{F}^{[0]}_{22}\mathscr{A}_{2222} - \overline{F}^{[0]}_{22}\overline{F}^{[0]}_{11}\mathscr{A}_{2211}\\
&= \left(\overline{F}^{[0]}_{22}\right)^2\left(\mathscr{A}_{2222} - \mathscr{A}_{2211}\overline{F}^{[0]}_{11}\Big/\overline{F}^{[0]}_{22}\right)\\
&= \left(\overline{F}^{[0]}_{22}\right)^2\delta\overline{P}^{[3,0]}_{22}\Big/\delta\overline{F}^{[3]}_{22},
\end{aligned}
\tag{B.3}
$$

and

$$
\begin{aligned}
\mathscr{A}^0_{1111} - \mathscr{A}^0_{2211} &= \overline{F}^{[0]}_{11}\overline{F}^{[0]}_{11}\mathscr{A}_{1111} - \overline{F}^{[0]}_{22}\overline{F}^{[0]}_{11}\mathscr{A}_{2211}\\
&= \left(\overline{F}^{[0]}_{11}\right)^2\left(\mathscr{A}_{1111} - \mathscr{A}_{2211}\overline{F}^{[0]}_{22}\Big/\overline{F}^{[0]}_{11}\right)\\
&= \left(\overline{F}^{[0]}_{11}\right)^2\delta\overline{P}^{[3,0]}_{11}\Big/\delta\overline{F}^{[3]}_{11},
\end{aligned}
\tag{B.4}
$$

where $\delta\overline{P}^{[3,0]}_{ii} = \overline{P}_{ii}(\overline{\mathbf{F}}^{[3]}, \overline{\mathbf{H}}^{[0]}) - \overline{P}_{ii}(\overline{\mathbf{F}}^{[0]}, \overline{\mathbf{H}}^{[0]})$, no summation.

References

[1] Abbott JJ, Ergeneman O, Kummer MP, Hirt AM, Nelson BJ. Modeling magnetic torque and force for controlled manipulation of soft-magnetic bodies. IEEE Trans Robotics 2007;23(6):1247–52.
[2] Babaee S, Viard N, Wang P, Fang NX, Bertoldi K. Harnessing deformation to switch on and off the propagation of sound. Adv Mater 2016;28(8):1631–5.
[3] Bednarek S. The giant magnetostriction in ferromagnetic composites within an elastomer matrix. Applied Physics A: Mater Sci Process 1999;68(1):63–7.
[4] Bertoldi K, Boyce MC. Mechanically triggered transformations of phononic band gaps in periodic elastomeric structures. Phys Rev B 2008;77(5):052105.
[5] Bertoldi K, Boyce MC, Deschanel S, Prange S, Mullin T. Mechanics of deformation-triggered pattern transformations and superelastic behavior in periodic elastomeric structures. J Mech Phys Solids 2008;56(8):2642–68.
[6] Bertoldi K, Gei M. Instabilities in multilayered soft dielectrics. J Mech Phys Solids 2011;59:18–42.
[7] Biot MA. Mechanics of incremental deformations. New-York: John Wiley and Sons; 1965.
[8] Brigadnov IA, Dorfmann A. Mathematical modeling of magneto-sensitive elastomers. Int J Solids Struct 2003;40:4659–74.
[9] Budday S, Andres S, Walter B, Steinmann P, Kuhl E. Wrinkling instabilities in soft bilayered systems. Phil Trans R Soc 2017;A 375(2093):20160163.
[10] Bustamante R, Dorfmann A, Ogden R. Universal relations in isotropic nonlinear magnetoelasticity. Q J Mech Appl Math 2006;59:435–50.
[11] Bustamante R, Merodio J. On simple constitutive restrictions for transversely isotropic nonlinearly elastic materials and isotropic magneto-sensitive elastomers. J Eng Math 2010;68(1):15–26.
[12] Ciambella J, Stanier DC, Rahatekar SS. Magnetic alignment of short carbon fibres in curing composites. Compos Part B Eng 2017;109:129–37.
[13] Cohen N, Menzel A, deBotton G. Towards a physics-based multiscale modelling of the electro-mechanical coupling in electro-active polymers. Proc R Soc A 2016;472(2186).
[14] Danas K, Triantafyllidis N. Instability of a magnetoelastic layer resting on a non-magnetic substrate. J Mech Phys Solids 2014;69:67–83.
[15] Deng H, Gong X, Wang L. Development of an adaptive tuned vibration absorber with magnetorheological elastomer. Smart Mater. Struct 2006;15: N111–6.
[16] Destrade M, Ogden RW. On magneto-acoustic waves in finitely deformed elastic solids. Math Mech Solids 2011;16:594–604.
[17] Diguet G, Beaugnon E, Cavaillé J. Shape effect in the magnetostriction of ferromagnetic composite. J Magnetism Magnetic Mater 2010;322(21): 3337–41.
[18] Dorfmann A, Ogden R. Nonlinear magnetoelastic deformations. Q J Mech Appl Math 2004a;57(4):599–622.
[19] Dorfmann A, Ogden R. Nonlinear magnetoelastic deformations of elastomers. Acta Mech 2004b;167(1–2):13–28.
[20] Dorfmann A, Ogden RW. Nonlinear magnetoelastic deformations. Q J Mech Appl Math 2004c;57:599–622.
[21] Dorfmann A, Ogden RW. Some problems in nonlinear magnetoelasticity. Z Angew Math Phys 2005;56:718–45.
[22] Dorfmann A, Ogden RW. Nonlinear electroelastostatics: incremental equations and stability. Int J Eng Sci 2010;48:1–14.
[23] Farshad M, Le Roux M. A new active noise abatement barrier system. Polym Test 2004;23:855–60.
[24] Galipeau E, Rudykh S, deBotton G, Ponte Castañeda P. Magnetoactive elastomers with periodic and random microstructures. Int J Solids Struct 2014;51: 3012–24.
[25] Gao C, Li Y. Tuning the wrinkling patterns of an interfacial/coating layer via a regulation interphase. Int J Solids Struct 2017;104:92–102.

[26] Geymonat G, Müller S, Triantafyllidis N. Homogenization of nonlinearly elastic materials, microscopic bifurcation and macroscopic loss of rank-one convexity. Arch Ration Mech Anal 1993;122:231–90.
[27] Ginder JM, Clark SM, Schlotter WF, Nichols ME. Magnetostrictive phenomena in magnetorheological elastomers. Int J Mod Phys B 2002;16:2412–8.
[28] Ginder JM, Schlotter WF, Nichols ME. Magnetorheological elastomers in tunable vibration absorbers. Proc SPIE 2001;4331:103.
[29] Guan X, Donga X, Ou J. Magnetostrictive effect of magnetorheological elastomer. J Magn Magn Mat 2008;320:158–63.
[30] Haldar K, Kiefer B, Menzel A. Finite element simulation of rate-dependent magneto-active polymer response. Smart Mater Struct 2016;25(10):104003.
[31] Hill R. On constitutive macro-variables for heterogeneous solids at finite strain. Proc R Soc Lond A 1972;326:131–47.
[32] Hill R, Hutchinson JW. Bifurcation phenomena in the plane tension test. J Mech Phys Solids 1975;23:239–64.
[33] Hoang N, Zhang N, Du H. An adaptive tunable vibration absorber using a new magnetorheological elastomer for vehicular powertrain transient vibration reduction. Smart Mater. Struct 2011;20:015019.
[34] Javili A, Chatzigeorgiou G, Steinmann P. Computational homogenization in magneto-mechanics. Int J Solids Struct 2013;50(25–26):4197–216.
[35] Jolly MR, Carlson JD, Munoz BC. A model of the behaviour of magneto-rheological materials. Smart Mater. Struct 1996;5:607–14.
[36] Kankanala SV, Triantafyllidis N. Magnetoelastic buckling of a rectangular block in plane strain. J Mech Phys Solids 2008;56:1147–69.
[37] Keip M-A, Rambausek M. Computational and analytical investigations of shape effects in the experimental characterization of magnetorheological elastomers. Int J Solids Struct 2017. https://doi.org/10.1016/j.ijsolstr.2017.04.012.
[38] Keip M, Steinmann P, Schröder J. Two-scale computational homogenization of electro-elasticity at finite strains. Comput Methods Appl Mech Eng 2014;278:62–79.
[39] Labusch M, Etier M, Lupascu DC, Schröder J, Keip M-A. Product properties of a two-phase magneto-electric composite: synthesis and numerical modeling. Comput Mech 2014;54(1):71–83.
[40] Lanotte L, Ausanio G, Iannotti V, Luponio Jr C. Influence of particle preorientation on elastomagnetic effect in a composite material of ellipsoidal ni microparticles in a silicone matrix. Appl Phys A 2003;77(7):953–8.
[41] Lerner AA, Cunefare KA. Performance of mre-based vibration absorbers. J Intelligent Material Syst Struct 2008;19:551–63.
[42] Li Y, Kaynia N, Rudykh S, Boyce MC. Wrinkling of interfacial layers in stratified composites. Adv Eng Mater 2013;15(10):921–6.
[43] Melnikov A, Ogden RW. Finite deformations of an electroelastic circular cylindrical tube. Z für Angew Math Phys 2016;67(6):140.
[44] Merodio J, Ogden R. Remarks on instabilities and ellipticity for a fiber-reinforced compressible nonlinearly elastic solid under plane deformation. Quart Appl Math 2005;63(2):325–33.
[45] Merodio J, Ogden RW. Material instabilities in fiber-reinforced nonlinearly elastic solids under plane deformation. Archives Mech (IPPT) 2002;54:525–52.
[46] Metsch P, Kalina KA, Spieler C, Kästner M. A numerical study on magnetostrictive phenomena in magnetorheological elastomers. Comput Mater Sci 2016;124:364–74.
[47] Michel JC, Lopez-Pamies O, Castañeda PP, Triantafyllidis N. Microscopic and macroscopic instabilities in finitely strained porous elastomers. J Mech Phys Solids 2007;55:900–38.
[48] Mullin T, Deschanel S, Bertoldi K, Boyce MC. Pattern transformation triggered by deformation. Phys Rev Lett 2007;99(8):84301.
[49] Ogden RW. Nonlinear elasticity and fibrous structure in arterial wall mechanics, lecture notes for summer school on modeling and computation in biomechanics. Austria: Graz University of Technology; 2008.
[50] Otténio M, Destrade M, Ogden R. Incremental magnetoelastic deformations, with application to surface instability. J Elast 2008;90:19–42.
[51] Ponte Castañeda P, Galipeau E. Homogenization-based constitutive models for magnetorheological elastomers at finite strain. J Mech Phys Solids 2011;59:194–215.
[52] Rudykh S, Bertoldi K. Stability of anisotropic magnetorheological elastomers in finite deformations: a micromechanical approach. J Mech Phys Solids 2013;61:949–67.
[53] Rudykh S, Bhattacharya K, deBotton G. Multiscale instabilities in soft heterogeneous dielectrics. Proc R Soc A 2014;470:20130618.
[54] Rudykh S, Boyce M. Transforming wave propagation in layered media via instability-induced interfacial wrinkling. Phys Rev Lett 2014;112:034301.
[55] Rudykh S, deBotton G. Stability of anisotropic electroactive polymers with application to layered media. Z Angew Math Phys 2011;62:1131–42.
[56] Rudykh S, deBotton G. Instabilities of hyperelastic fiber composites: micromechanical versus numerical analyses. J Elast 2012;106:123–47.
[57] Rudykh S, Lewinstein A, Uner G, deBotton G. Analysis of microstructural induced enhancement of electromechanical coupling in soft dielectrics. Appl Phys Lett 2013;102:151905.
[58] Schröder J, Keip M-A. Two-scale homogenization of electromechanically coupled boundary value problems. Comput Mech 2012;50(2):229–44.
[59] Slesarenko V, Rudykh S. Harnessing viscoelasticity and instabilities for tuning wavy patterns in soft layered composites. Soft Matter 2016;12:3677–82.
[60] Slesarenko V, Rudykh S. Microscopic and macroscopic instabilities in hyperelastic fiber composites. J Mech Phys Solids 2017;99:471–82.
[61] Stanier DC, Ciambella J, Rahatekar SS. Fabrication and characterisation of short fibre reinforced elastomer composites for bending and twisting magnetic actuation. Compos Part A Appl Sci Manuf 2016;91:168–76.
[62] Tian TF, Li WH, Deng YM. Sensing capabilities of graphite based mr elastomers. Smart Mater. Struct 2011;20:025022.
[63] Triantafyllidis N, Maker BN. On the comparison between microscopic and macroscopic instability mechanisms in a class of fiber-reinforced composites. J Appl Mech, Trans ASME 1985;52:794–800.
[64] Truesdell C, Toupin R. The classical field theories, Handbuch der Physik,, vol. III. Berlin: Springer; 1960.
[65] Vu DK, Steinmann P. Nonlinear electro- and magneto-elastostatics: material and spatial settings. Int J Solids Struct 2007;44(24):7891–905.